

The Defect Chemistry of Carbon Frameworks for Regulating the Lithium Nucleation and Growth Behaviors in Lithium Metal Anodes

Xia-Xia Ma, Xiang Chen, Yun-Ke Bai, Xin Shen, Rui Zhang, and Qiang Zhang*

Carbon materials have been widely considered as the frameworks in lithium (Li) metal anodes due to their lightweight, high electrical conductivity, and large specific surface area. Various heteroatom-doping strategies have been developed to enhance the lithiophilicity of carbon frameworks, thus rendering a uniform Li nucleation in working Li metal batteries. The corresponding lithiophilicity chemistry of doping sites has been comprehensively probed. However, various defects are inevitably introduced into carbon materials during synthesis and their critical role in regulating Li nucleation and growth behaviors is less understood. In this contribution, the defect chemistry of carbon materials in Li metal anodes is investigated through first-principles calculations. The binding energy towards a Li atom and the critical current density are two key descriptors to reveal the defect chemistry of carbon materials. Consequently, a diagram of designing carbon frameworks with both high lithiophilicity and a large critical current density is built, from which the Stone–Wales defect is predicted to possess the best performance for delivering a uniform Li deposition. This work uncovers the defect chemistry of carbon frameworks and affords fruitful insights into defect engineering for achieving dendrite-free Li metal anodes.

With the rapid increase of the global population and energy demands, building high-energy-density batteries becomes more and more important for constructing sustainable energy systems.^[1,2] Lithium (Li) metal, with an ultrahigh theoretical specific capacity (3860 mAh g⁻¹) and a very low electrochemical potential (−3.040 V versus the standard hydrogen electrode), is a promising anode material for constructing high-energy-density batteries.^[3–9] However, the application of Li metal anodes is faced with serious challenges, such as the formation of notorious Li dendrites, the low Coulombic efficiency, and the infinite relative volume change during cycling.^[10–13] Especially, Li dendrites not only induce the consumption of electrolyte and the formation of “dead Li” during the subsequent plating/stripping

cycles, finally resulting in capacity fading, but also can penetrate through the separator, causing the short circuit and safety hazards.^[8,14,15]

Constructing a composite Li metal anode framework has been strongly considered to both retard the formation of Li dendrites and reduce the volume expansion.^[14,16–20] Among various host candidates, carbon materials, including carbon nanotubes,^[21] graphene,^[22,23] graphite paper,^[24] graphene balls,^[25] and carbon nanospheres,^[26,27] have been widely probed due to their lightweight, high electrical conductivity, and large specific surface area. Pure carbon can only afford a weak interaction with Li metal, which renders a high specific interfacial energy and a large nucleation barrier. Therefore, heteroatom-doping strategies are often adopted to enhance the electrochemical performance of carbon hosts, and the working mechanism of doping sites is comprehensively investigated.^[3,22,28] For instance, Foroozan

et al. constructed a 3D conformal graphene oxide nanosheet to effectively regulate uniform Li deposition.^[29] Through scanning electron microscopy and optical observations, they demonstrated that a dense and uniform deposition of Li could be achieved by the 3D conformal graphene oxide nanosheet.

Defects are almost inevitably introduced during the synthesis of various carbon materials, especially the heteroatom-doped carbon.^[3,30–32] More importantly, carbon atoms in defects often play as the active sites in surface reactions as the unsaturated-coordination nature affords them a stronger interaction with reactants than the other atoms. In Li metal batteries, defective graphene was reported to increase the Coulombic efficiency and prevent dendritic growth.^[33,34] However, Liu et al. reported that pristine graphene (PG) yields state-of-the-art electrochemical performance with the post cycled metal surface, which is relatively smoother and more dendrite-free than defective graphene.^[35] The different results induced by defects are originated from various defect types. Therefore, it is very important to understand the fundamental role of various defects in regulating the Li nucleation. If a comprehensive and deep understanding of defect chemistry can be built, highly lithiophilic carbon materials can be rationally designed through both defect engineering and heteroatom-doping strategies.

Dr. X.-X. Ma, Dr. X. Chen, Y.-K. Bai, X. Shen, Dr. R. Zhang, Prof. Q. Zhang
Beijing Key Laboratory of Green Chemical Reaction Engineering and Technology
Department of Chemical Engineering
Tsinghua University
Beijing 100084, China
E-mail: zhang-qiang@mails.tsinghua.edu.cn

 The ORCID identification number(s) for the author(s) of this article can be found under <https://doi.org/10.1002/smll.202007142>.

DOI: 10.1002/smll.202007142

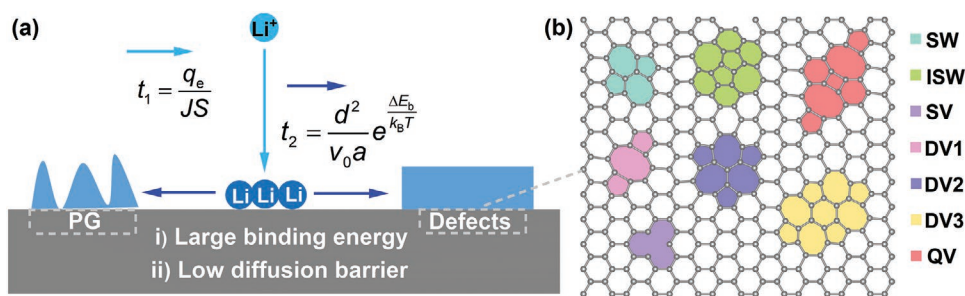


Figure 1. Schematic of Li nucleation and growth on carbon frameworks. a) The deposition of Li ions on PG and graphene with various defects. b) Modeling of graphene with defects: SW, ISW, SV, DV1, DV2, DV3, and QV.

In this contribution, the defect chemistry in carbon materials is investigated based on 2D graphene models through first-principles calculations. Seven kinds of defects are considered, among which three models exhibit both a larger binding energy with a Li atom and a lower Li atom diffusion barrier across the defects than PG. The large binding energy is beneficial to reduce the nucleation barrier and the low diffusion barrier contributes to a 2D Li deposition morphology, which are both helpful to resist the growth of Li dendrites and render a uniform Li deposition. This work reveals the defect chemistry in carbon materials and affords a fruitful insight into the rational design of high-performance frameworks in Li metal anodes.

The heterogeneous nucleation and the following growth of Li metal on carbon frameworks are highly dependent on both the lithiophilicity of the nucleation sites and the diffusion barrier of Li atom on the carbon plane (Figure 1a). A highly lithiophilic site can induce a large binding energy toward Li, which is beneficial to reduce both the desolvation barrier of Li ions and the interfacial energy between carbon and Li metal. The latter is a key parameter to control the contact angle between the host and the newly formed phase, consequently regulating the heterogeneous nucleation barrier. According to the classical nucleation theory, a lower interfacial energy renders a smaller contact angle and a much more reduced heterogeneous nucleation barrier comparing with homogeneous nucleation barrier.^[36] Besides, the diffusion properties have an obvious influence on the Li deposition progress.^[37–40] An uneven distribution of lithiophilic sites is unable to ensure a uniform deposition as Li metal prefers to grow on the nucleation sites. A low diffusion barrier can help the initial deposited Li atoms move to the whole carbon plane and produce a smooth deposition morphology.

In order to evaluate the role of carbon with defects in regulating Li nucleation and growth behaviors, seven kinds of defects are probed based on a 2D single-layered graphene model (Figure 1b). Specifically, Stone–Wales (SW), inversion Stone–Wales (ISW), single vacancy (SV), three double vacancies (DV1, DV2, and DV3), and quadra vacancies (QV) defects are considered. The SW defects have been widely found in graphene,^[41] carbon nanotubes,^[42] and fullerenes.^[43] Meanwhile, both SV and double vacancies are widely reported in experiments through a high-resolution transmission electron microscope (HRTEM).^[44] The ISW is one forecasting defects by density functional theory calculations.^[45] In addition, the QV defect is also considered to explore the influence of vacancy number.

Among them, the SW defect is obtained through rotating the C–C bond 90° with respect to the midpoint of it, which includes two adjacent heptagonal carbon rings (C7) and two adjacent pentagonal carbon rings (C5). The SV defect is created by removing one carbon atom in graphene, which causes dangling bonds and increases the local polarity. Double vacancies are created by removing adjacent two carbon atoms, namely, DV1. The DV1 includes two C5 and one octagonal carbon ring (C8). Rotating the bond in C8 of DV1 can create DV2, which includes three C7 and three C5. Furthermore, rotating the bond in C7 of DV2 can create DV3, which includes four C7, four C5, and hexagonal carbon ring (C6). The QV is created by removing four carbon atoms, which includes one tetragonal carbon ring (C4), two C5, two C6, and two C8. In addition to vacancy defects, adding a carbon atom defect is also considered, namely, ISW defects. Different from the above defects, the ISW defect destructs the planarity of graphene, producing a “hat” shape. The top of the “hat” includes two C5 and the bottom of the “hat” includes four C6 and two C7.

The formation of defects in carbon is strongly related to its formation energy level. Among the seven considered defects, the SW defect has the lowest formation energy of 0.14 eV prim^{-1} . (Figure 2a), which agrees with tremendous reports of its thermodynamic stability.^[46] Besides, the SW rearrangement has important implications for the chemical, electrical, and mechanical properties of carbon materials.^[43] On the contrary, the QV defect presents the largest formation energy of 0.40 eV prim^{-1} , which is attributed to the relatively unstable C4 structure in the carbon plane. The formation energies of the other defects are about 0.20 eV prim^{-1} . Relative low formation energy indicates these defects can be formed in experiments. Indeed, SW, SV, and three double vacancies have been widely reported in experiments.^[41,42,44]

The graphene models are further allowed to interact with a Li atom to determine the binding energy, which is a key parameter to describe the lithiophilicity.^[3] For each model, all possible adsorption sites around the defects are considered and the maximum binding energy of each defect is used for further comparisons (Figure 2, Figures S1 and S2, Supporting Information). Generally, C5, C7, and C8 sites have a larger binding energy with a Li atom than the C6 site, showing great potential of increasing the lithiophilicity of carbon materials through defect engineering. For instance, the binding energies of the C5, C8, and C6 sites in DV1 defect are -2.08 , -2.27 , and -1.95 eV, respectively. In the C6 site, the carbon atom forms three σ bonds with its nearest neighbor carbon atoms and a delocal-

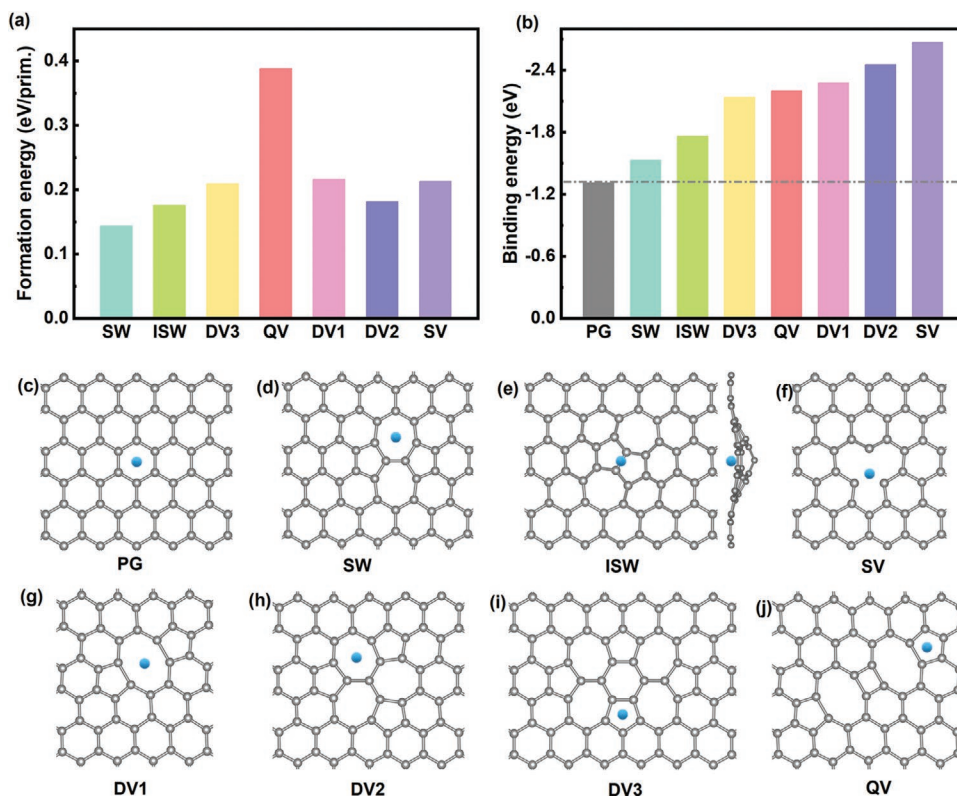


Figure 2. Modeling and summary of graphene defect formation energy and Li binding energy. a) The defect formation energy of graphene. Prim is the abbreviation of primitive cell and one primitive cell has two carbon atoms. b) The binding energy between a Li atom and defective graphene. c–j) The optimized interaction structures of a Li atom and defective graphene. The Li and carbon atoms are marked as blue and gray, respectively.

ized π bond. The saturated coordination structure of the carbon results in a relatively weak electrostatic interaction between the Li atom and the C6 ring. However, the situation of the carbon atoms in defects is very different. They are often coordination-unsaturated and even have a single electron or an electron pair, which can induce a strong bonding with a Li atom. Specifically, the binding energies are -1.53 , -1.48 , -1.41 , and -1.29 eV for the nearest C7, C5, and C6 of the SW defect and the second nearest C6 of the SW defect, respectively (Figure S1b1–4, Supporting Information). As a result, Li prefers C5 and C7 than C6 around the SW defect. Similarly, the binding energies of the C5 and C8 sites are more negative than the C6 sites in DV1, DV2, DV3, and QV defects. Besides, the Li atom is adsorbed just above the vacancy in the SV defect (Figure S1c1, Supporting Information). ISW defect can form a structure like a hat and a Li atom prefers to be trapped in the carbon hole (Figure S1h4, Supporting Information).

The most stable absorption geometrical structures and corresponding binding energies for each defect are summarized in Figure 2. The binding energies of PG, SW, SV, DV1, DV2, DV3, QV, and ISW defects are -1.31 , -1.53 , -2.67 , -2.27 , -2.45 , -2.14 , -2.20 , and -1.76 eV, respectively. All defects have a more negative binding energy than PG, indicating that introducing any of these defects can improve the lithiophilicity of carbon hosts. The strong interaction between the Li atom and defective sites can speedily break the Li bond between a Li-ion and electrolyte solvents or anions, which can reduce the nucleation and deposition overpotentials.^[47] Among various defects, the SV has the most

negative binding energy (-2.67 eV), which is two times PG (-1.31 eV). The strong interaction between a Li atom and SV can be explained by the binding bonds in the SV, which can form Li–C bonds. The Li–C bond length in SV (2.08 Å) is similar to that in organolithium molecules (2.00 – 2.18 Å) but much shorter than the distance between the Li and C atoms in PG (2.26 Å).

Although the SV has the most negative binding energy among various defects, it has only one most stable adsorption sites. Meanwhile, SW, DV2, and DV3 defects have two C7 (Figure 2d), three C7 (Figure 2h), and four C5 (Figure 2i) adsorption sites, respectively, which all exhibit larger binding energies than the C6 sites in PG. Therefore, SW, DV2, and DV3 defects have more nucleation sites than SV when their defect densities are the same. Enough and uniform nucleation sites are necessary to guarantee a smooth Li metal deposition.

Bader charge and differential charge density analyses are further performed to probe the strong interaction between Li and graphene with specific defects (Figure 3). PG is a non-polar material and the Bader charge of all carbon atoms is near zero (Figure 3a). The introduction of defects can only cause a slight charge fluctuation in the carbon plane due to the lacking of strong electron-donating or electron-withdrawing functional groups (Figure 3b,c). When a Li atom is adsorbed on the graphene, an obvious charge transfer of about $0.9 e^-$ from the Li to carbon is observed, which is a necessary requirement for achieving a large binding energy.^[3,36] Specifically, the charge transfers of PG, SW, and SV are 0.91 , 0.91 , and $0.90 e^-$ (Figure 3d–f), respectively. The charge transfers of other defects

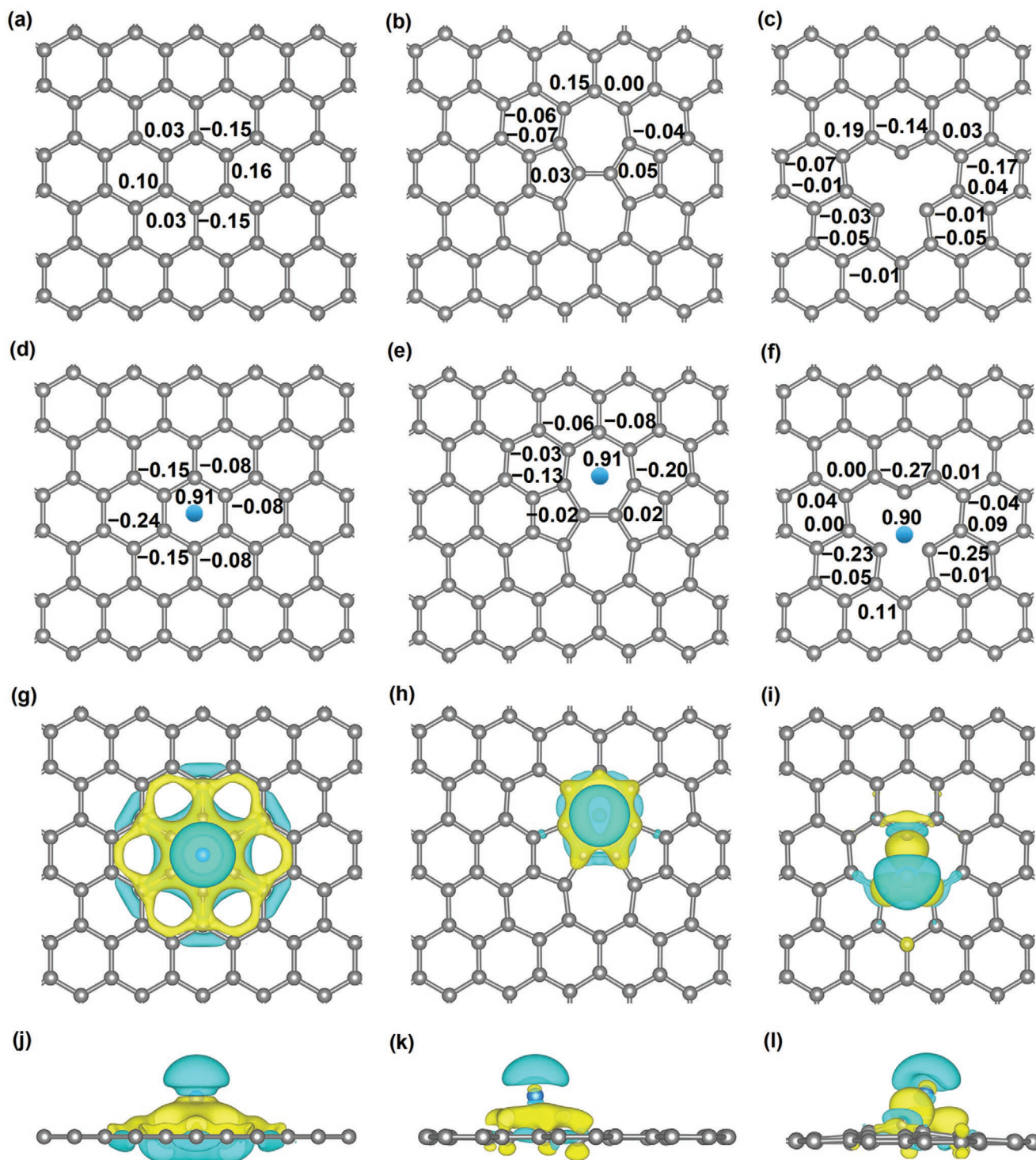


Figure 3. The Bader charge of PG and graphene with defects. The Bader charge distribution before and after adsorption, and the corresponding top and side views of differential charge density of Li adsorption site of a,d,g,j) PG, b,e,h,k) SW, and c,f,i,l) SV, respectively. The black numbers are the Bader charge of the nearest atoms. The yellow and cyan surfaces correspond to the charge gain and lost regions, respectively (isovalue, $0.0025 \text{ e}^- \text{ Bohr}^{-3}$). The Li and carbon atoms are marked as blue and gray, respectively.

are also about 0.90 e^- (Figure S3, Supporting Information). Besides, the transferred charge is mainly distributed around the adsorption sites. The differential charge density intuitively

presents the charge transfer between the Li atom and carbon plane (Figure 3g–i). More importantly, a strong Li–C bond is formed in the SV defect, resulting in a large binding energy.

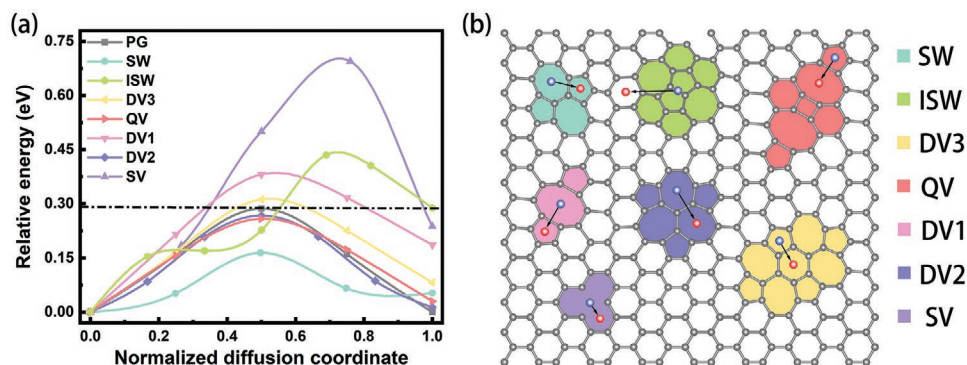


Figure 4. The Li diffusion pathway and barrier on graphene. a) Li diffusion barrier on graphene with and without defects. b) Li diffusion pathway on graphene with different defects. The Li and carbon atoms are marked as blue or red and gray, respectively. Blue and red Li atoms correspond to the initial and final diffusion sites.

A highly lithiophilic anode framework can only ensure the uniform deposition at a small current density while kinetic factors play an important role under a large current density. For example, Chen and co-workers reported that Li dendrites grow when the Li plating rate becomes larger than the Li chemical diffusion rate.^[48] Meanwhile, it is reported that the Li diffusion as the rate-determining step induces the dendrites growth.^[49] According to Sand's time model, a larger current density results in a smaller Sand's time and easier dendritic growth.^[50] Therefore, the Li diffusion barrier on the anode framework has an important role in regulating the Li deposition behaviors at a large current density.

The Li diffusion barrier across the defect sites on graphene is calculated by the climbing image Nudged Elastic Band method and the results are summarized in Figure S4, Supporting Information. All possible diffusion pathways are considered and the optimal ones are used for comparisons (Figure 4 and Figure S5, Supporting Information). The diffusion barriers of SW, DV2, and QV are 0.16, 0.27, and 0.26 eV, respectively, which are lower than that of PG (0.29 eV). The low diffusion barrier affords the graphene frameworks with a large diffusivity, which is beneficial to improve the Li deposition behavior under a large current density. On the contrary, the diffusion barriers of the other defects are higher than that of PG. Especially, the SV has the largest diffusion barrier (0.69 eV), indicating that the absorbed Li atoms can only be trapped in vacancy sites and hardly move to neighbor sites. The SV defect with strong lithiophilicity and low diffusivity can be used to explain the experimental observation that defective graphene is better electrochemically wetted by Li than PG at the first cycle, but the PG renders smooth and dendrite-free metal surface than the defective graphene during the following cycles.^[35]

According to the deposition–diffusion model (Details in, Table S1, Supporting Information), a critical current density is defined as the current density when the Li deposition rate is equal to the Li diffusion rate on anode framework. The diffusion rate is larger than the deposition rate below the critical current density and the deposited Li can be covered on the whole anode smoothly. On the contrary, Li prefers to grow in vertical quickly and thus results in a dendritic morphology when the diffusion rate is much smaller than the deposition rate. Therefore, the critical current density is another important

parameter for considering the carbon anode performance. The critical current density of SW, DV2, and QV are 3.68×10^7 , 4.37×10^5 , and 1.17×10^6 mA cm⁻², which are 106.98, 1.27, and 3.40 times as much as that of PG (3.44×10^5 mA cm⁻²), respectively. The theoretical value is much larger than experimental current densities, indicating carbon materials with these kinds of defects can resist the Li dendritic growth effectively. Besides, the critical current densities of ISW, DV1, and DV3 are 3.15×10^2 , 1.04×10^4 , and 1.89×10^5 mA cm⁻², respectively. However, they are smaller than that of PG but much larger than the experimental value. Unfortunately, the SV defects significantly reduce the critical current density to 7.90×10^{-2} mA cm⁻², which is smaller than most experimental current densities. Therefore, the SV can cause a serious dendritic growth from the kinetic viewpoint although it has a good lithiophilicity.

Simultaneously, the difference between theoretical and experimental critical current densities should be clarified. The experimental current density is calculated based on the anode surface area, which can be 1000 times smaller than the surface area of porous carbon frameworks. The large specific surface area can explain the high value of theoretical critical current density. Besides, the Li-ion diffusivity in electrolytes is not considered but has an obvious influence under a large current density according to Sand's time model. As a result, it is possible to form Li dendrites below the critical current density. However, these disadvantages do not prevent the critical current density to afford deep insights into understanding the role of defects in regulating Li deposition.

In order to design delicate graphene frameworks through defect engineering that can work at a wide range of current densities, a diagram is built with an overall consideration of both lithiophilicity and critical current density (Figure 5). The diagram can be divided into four regions according to the binding energy and the critical current density of PG. For instance, in the right–top region, which is marked with light-yellow, the defects have both a larger binding energy and critical current density than PG. The large binding energy can decrease the Li nucleation barrier and the large critical current density can ensure the uniform deposition morphology under large current densities. Accordingly, SW, DV2, and QV defects are supposed to improve the anode performances of carbon frameworks.

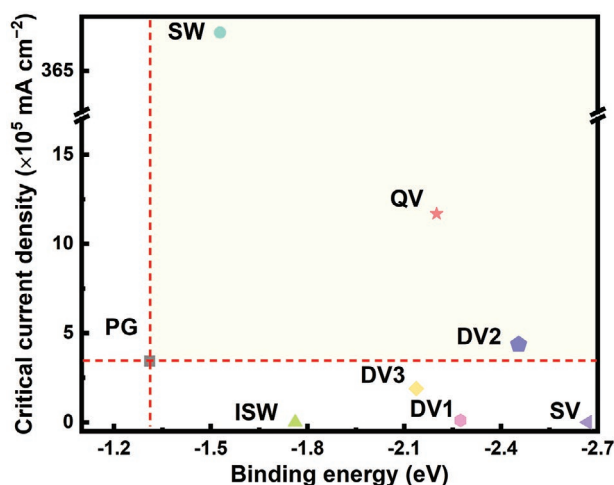


Figure 5. The diagram of designing high-performance carbon frameworks for Li metal anodes. SW, QV, and DV2 defects located in light yellow areas possess high lithiophilicity and large critical current density, which are ideal sites for Li nucleation and uniform growth.

Although defects widely existed in carbon materials, it is extremely hard to achieve a precise synthesis of carbon with only one kind of defect in experiments currently. It is possible to enrich one or several kinds of defects through post-processing, such as ball milling, plasma technique, chemical etching, high-temperature annealing, and templated-based carbonization.^[51–53] For example, the SW defect can be introduced through electron beam irradiation, which can only rotate one C–C bond but does not knock out a carbon atom under a controlled electron beam irradiation energy.^[46] Yao and coauthors reported the directional synthesis of definitive defect configurations converted from corresponding specific nitrogen doping sites, which can be much easier to be achieved in experiments. Specifically, graphitic, pyridinic, and pyrrolic nitrogen doping sites can produce divacancy, separate pentagon, and adjacent pentagons defects, respectively, by removing the heteroatoms through both electron beam irradiation and high-temperature annealing.^[51] It should be noted that extremely violent methods should be avoided to prevent the production of inappropriate high-formation-energy SV defects.^[53]

In conclusion, the role of defects in graphene in regulating Li nucleation and growth behaviors is revealed from two aspects of Li binding energy and diffusion barrier. The defects with C5, C7, or C8 sites have larger binding energies than PG, which is beneficial to reduce the Li nucleation barrier and promote uniform Li depositions. Only SW, DV2, and QV defects have a low diffusion barrier than PG, which increases the critical current density and therefore improves the anode performance at the large current density. Finally, a diagram is proposed, giving rational guidance for constructing highly lithiophilic carbon frameworks by defect engineering, from which the SW defect is predicted to possess the best performance for delivering a uniform Li deposition. This work reveals the defect chemistry of carbon materials, and further proposes reliable strategies to construct high-performance carbon frameworks for dendritic-free Li metal anodes.

Supporting Information

Supporting Information is available from the Wiley Online Library or from the author.

Acknowledgements

This work was supported by the Beijing Municipal Natural Science Foundation (Z20J00043), National Natural Scientific Foundation of China (21825501 and 21808121), the National Key Research and Development Program (2016YFA0202500 and 2016YFA0200102), and Tsinghua University Initiative Scientific Research Program. The authors acknowledge the support from Tsinghua National Laboratory for Information Science and Technology for theoretical simulations.

Conflict of Interest

The authors declare no conflict of interest.

Data Availability Statement

Data available on request from the authors.

Keywords

carbon frameworks, critical current density, defect chemistry, lithiophilicity, lithium metal anodes

Received: November 12, 2020

Revised: January 23, 2021

Published online:

- [1] Y. Liang, C. Z. Zhao, H. Yuan, Y. Chen, W. Zhang, J. Q. Huang, D. Yu, Y. Liu, M. M. Titirici, Y. L. Chueh, H. Yu, Q. Zhang, *InfoMat* **2019**, *1*, 6.
- [2] S. Chu, A. Majumdar, *Nature* **2012**, *488*, 294.
- [3] X. Chen, X. R. Chen, T. Z. Hou, B. Q. Li, X. B. Cheng, R. Zhang, Q. Zhang, *Sci. Adv.* **2019**, *5*, eaau7728.
- [4] R. Xu, X.-B. Cheng, C. Yan, X.-Q. Zhang, Y. Xiao, C.-Z. Zhao, J.-Q. Huang, Q. Zhang, *Matter* **2019**, *1*, 317.
- [5] X.-Q. Zhang, X. Chen, X.-B. Cheng, B.-Q. Li, X. Shen, C. Yan, J.-Q. Huang, Q. Zhang, *Angew. Chem., Int. Ed.* **2018**, *57*, 5301.
- [6] R. Wang, W. Cui, F. Chu, F. Wu, *J. Energy Chem.* **2020**, *48*, 145.
- [7] P. Shi, X. B. Cheng, T. Li, R. Zhang, H. Liu, C. Yan, X. Q. Zhang, J. Q. Huang, Q. Zhang, *Adv. Mater.* **2019**, *31*, 1902785.
- [8] X. B. Cheng, R. Zhang, C. Z. Zhao, Q. Zhang, *Chem. Rev.* **2017**, *117*, 10403.
- [9] Y. X. Yao, X. Q. Zhang, B. Q. Li, C. Yan, P. Y. Chen, J. Q. Huang, Q. Zhang, *InfoMat* **2020**, *2*, 379.
- [10] P. Albertus, S. Babinec, S. Litzelman, A. Newman, *Nat. Energy* **2017**, *3*, 16.
- [11] H. Liu, X.-B. Cheng, J.-Q. Huang, S. Kaskel, S. Chou, H. S. Park, Q. Zhang, *ACS Mater. Lett.* **2019**, *1*, 217.
- [12] Y. Chen, Y. Luo, H. Zhang, C. Qu, H. Zhang, X. Li, *Small Methods* **2019**, *3*, 1800551.
- [13] X. Shen, X. Cheng, P. Shi, J. Huang, X. Zhang, C. Yan, T. Li, Q. Zhang, *J. Energy Chem.* **2019**, *37*, 29.

- [14] H. Zhao, D. Lei, Y.-B. He, Y. Yuan, Q. Yun, B. Ni, W. Lv, B. Li, Q.-H. Yang, F. Kang, J. Lu, *Adv. Energy Mater.* **2018**, *8*, 1800266.
- [15] D. Kang, K. Tang, J. Koh, W. Liang, J. P. Lemmon, *J. Energy Chem.* **2020**, *44*, 68.
- [16] B.-Q. Li, X.-R. Chen, X. Chen, C.-X. Zhao, R. Zhang, X.-B. Cheng, Q. Zhang, *Research* **2019**, *2019*, 4608940.
- [17] H. Wang, Y. Liu, Y. Li, Y. Cui, *Electrochem. Energ. Rev.* **2019**, *2*, 509.
- [18] L. Shen, P. Shi, X. Hao, Q. Zhao, J. Ma, Y. B. He, F. Kang, *Small* **2020**, *16*, 2000699.
- [19] K. Lin, T. Li, S. W. Chiang, M. Liu, X. Qin, X. Xu, L. Zhang, F. Kang, G. Chen, B. Li, *Small* **2020**, *16*, 2001784.
- [20] Y. Nan, S. Li, Y. Shi, S. Yang, B. Li, *Small* **2019**, *15*, 1903520.
- [21] Y. Wang, Y. Shen, Z. Du, X. Zhang, K. Wang, H. Zhang, T. Kang, F. Guo, C. Liu, X. Wu, W. Lu, L. Chen, *J. Mater. Chem. A* **2017**, *5*, 23434.
- [22] R. Zhang, X. R. Chen, X. Chen, X. B. Cheng, X. Q. Zhang, C. Yan, Q. Zhang, *Angew. Chem., Int. Ed.* **2017**, *56*, 7764.
- [23] T. Yang, L. Li, F. Wu, R. Chen, *Adv. Funct. Mater.* **2020**, *30*, 2002013.
- [24] Z. Huang, D. Kong, Y. Zhang, Y. Deng, G. Zhou, C. Zhang, F. Kang, W. Lv, Q.-H. Yang, *Research* **2020**, *2020*, 7163948.
- [25] S. Liu, A. Wang, Q. Li, J. Wu, K. Chiou, J. Huang, J. Luo, *Joule* **2018**, *2*, 184.
- [26] G. Zheng, S. W. Lee, Z. Liang, H.-W. Lee, K. Yan, H. Yao, H. Wang, W. Li, S. Chu, Y. Cui, *Nat. Nanotechnol.* **2014**, *9*, 618.
- [27] S. Ha, J. C. Hyun, J. H. Kwak, H. D. Lim, Y. S. Yun, *Small* **2020**, *16*, 2003918.
- [28] F. López-Urías, J. L. Fajardo-Díaz, A. J. Cortés-López, C. L. Rodríguez-Corvera, L. E. Jiménez-Ramírez, E. Muñoz-Sandoval, *Phys. Chem. Chem. Phys.* **2020**, *22*, 4533.
- [29] T. Foroozan, F. A. Soto, V. Yurkiv, S. Sharifi-Asl, R. Deivanayagam, Z. Huang, R. Rojjaee, F. Mashayek, P. B. Balbuena, R. Shahbazian-Yassar, *Adv. Funct. Mater.* **2018**, *28*, 1705917.
- [30] C. Tang, H. F. Wang, X. Chen, B. Q. Li, T. Z. Hou, B. Zhang, Q. Zhang, M. M. Titirici, F. Wei, *Adv. Mater.* **2016**, *28*, 6845.
- [31] Y. Zhang, L. Tao, C. Xie, D. Wang, Y. Zou, R. Chen, Y. Wang, C. Jia, S. Wang, *Adv. Mater.* **2020**, *32*, 1905923.
- [32] J. Yi, J. Chen, Z. Yang, Y. Dai, W. Li, J. Cui, F. Ciucci, Z. Lu, C. Yang, *Adv. Energy Mater.* **2019**, *9*, 1901796.
- [33] R. Mukherjee, A. V. Thomas, D. Datta, E. Singh, J. Li, O. Eksik, V. B. Shenoy, N. Koratkar, *Nat. Commun.* **2014**, *5*, 3710.
- [34] J. Jiang, Y. Zhang, Z. Li, Y. An, Q. Zhu, Y. Xu, S. Zang, H. Dou, X. Zhang, *J. Colloid Interface Sci.* **2020**, *567*, 75.
- [35] W. Liu, Y. Xia, W. Wang, Y. Wang, J. Jin, Y. Chen, E. Paek, D. Mitlin, *Adv. Energy Mater.* **2019**, *9*, 1802918.
- [36] X. Chen, Y.-K. Bai, X. Shen, H.-J. Peng, Q. Zhang, *J. Energy Chem.* **2020**, *51*, 1.
- [37] P. Zhu, X. Yang, X. Li, N. Sheng, H. Zhang, G. Zhang, J. Sha, *Dalton Trans.* **2020**, *49*, 79.
- [38] V. Pande, V. Viswanathan, *ACS Energy Lett.* **2019**, *4*, 2952.
- [39] Q. Yang, M. Cui, J. Hu, F. Chu, Y. Zheng, J. Liu, C. Li, *ACS Nano* **2020**, *14*, 1866.
- [40] C. Yan, H. Yuan, H. S. Park, J.-Q. Huang, *J. Energy Chem.* **2020**, *47*, 217.
- [41] J. C. Meyer, C. Kisielowski, R. Erni, M. D. Rossell, M. F. Crommie, A. Zettl, *Nano Lett.* **2008**, *8*, 3582.
- [42] K. Balasubramanian, M. Burghard, *J. Mater. Chem.* **2008**, *18*, 3071.
- [43] M. I. Heggie, G. L. Haffenden, C. D. Latham, T. Trevethan, *Philos. Trans. R. Soc., A* **2016**, *374*, 20150317.
- [44] A. Hashimoto, K. Suenaga, A. Gloter, K. Urita, S. Iijima, *Nature* **2004**, *430*, 870.
- [45] M. T. Lusk, L. D. Carr, *Phys. Rev. Lett.* **2008**, *100*, 175503.
- [46] F. Banhart, J. Kotakoski, A. V. Krasheninnikov, *ACS Nano* **2011**, *5*, 26.
- [47] X. Chen, Y. K. Bai, C. Z. Zhao, X. Shen, Q. Zhang, *Angew. Chem., Int. Ed.* **2020**, *132*, 11288.
- [48] Y. Chen, X. Dou, K. Wang, Y. Han, *Adv. Energy Mater.* **2019**, *9*, 1900019.
- [49] X. R. Chen, Y. X. Yao, C. Yan, R. Zhang, X. B. Cheng, Q. Zhang, *Angew. Chem., Int. Ed.* **2020**, *59*, 7743.
- [50] H. J. S. Sand, *Proc. Phys. Soc. London* **1899**, *17*, 496.
- [51] X. Wang, Y. Jia, X. Mao, L. Zhang, D. Liu, L. Song, X. Yan, J. Chen, D. Yang, J. Zhou, K. Wang, A. Du, X. Yao, *Chem* **2020**, *6*, 2009.
- [52] J. Zhu, S. Mu, *Adv. Funct. Mater.* **2020**, *30*, 2001097.
- [53] G. Lee, J. Kim, K. Kim, J. W. Han, *J. Vac. Sci. Technol. A* **2015**, *33*, 060602.